Chapter 19

Fabrication of Plasmonic Crystalline Thin Film of Titanium Nitride (TiN) by Pulsed Laser Deposition with Third Harmonic of Nd:YAG Laser and Its Spectroscopic Analyses

Yasushi Oshikane

Additional information is available at the end of the chapter

http://dx.doi.org/10.5772/67765

Abstract

The author has been engaged in the development of a novel optical fiber probe using scanning near-field optical microscope (SNOM) with an efficient, plasmonic and asymmetric Metal-Insulator-Metal (MIM) structure at the probe tip. As a metallic layer, titanium nitride (TiN), one of the alternative plasmonic materials, is selected. A pulsed laser deposition (PLD) is used to fabricate the film by high-power Nd:YAG laser. The PLDed films have been analyzed by X-ray diffractometer (XRD), UV-Vis/NIR spectrophotometer, scanning electron microscope (SEM), and X-ray photoelectron spectroscopy (XPS). Though most of previous PLD studies of TiN film used a titanium target with reactive gases, the study presented in this chapter has significant features of (1) a hot pressed target of crystalline TiN powder and (2) third harmonic of injection-seeded Nd:YAG laser which have temporally smoothed Gaussian with a constant pulse energy. The very first PLD process has succeeded to fabricate flat and dense films of a few hundred nanometers. The TiN film, which lustered like gold, indicated two peaks at 36.7° (111) and 42.6° (200) in XRD patterns that correspond to crystal structure of TiN. An elementary analysis of the TiN film has carried out using XPS, and appropriate spectra with chemical shifts were observed.

Keywords: alternative plasmonic material, titanium nitride (TiN), plasmonic thin film, pulsed laser deposition (PLD), crystalline thin film, third harmonic of pulsed Nd:YAG laser, X-ray diffractometer (XRD), electromagnetic FEM simulation, X-ray photoelectron spectroscopy (XPS)

1. Introduction

In the 1980s, basic and applied research regarding surface plasmon, which is a compression wave excited at boundary between metallic and insulating thin films and propagates along the boundary, was started. Propagation characteristics of the wave depend on combined complex dielectric constant of the two media, which form the boundary. The surface plasmon, which is locally excited at the medium surface, has been widely used in (1) a highly sensitive detection mechanism for an infinitesimal amount of element or molecule, (2) formation of highly intense point light source at the apex of scanning probe used in scanning near-field optical microscopes (SNOMs), and (3) localized intense fields at the surface of single tiny metallic particle as a highly sensitive detector or a strong illuminator.

(1) Surface plasmon resonance caused by the total internal reflection inside of a transparent insulator covered with metallic thin layer and (2) surface plasmon polarities excited in subwavelength structure consisting metallic and insulating thin films need appropriate materials including free electrons which might be oscillated by external electromagnetic of light. And response of the electrons to the light field must show negative real component in complex dielectric constant. As a result, noble metals, i.e., gold (Au) and silver (Ag), have been widely used for plasmonic research. A silver thin film is known as the best plasmonic material in the visible region but transubstantiates easily. Also silver is soft and does not have excellent adhesive power to the glass surface. Gold thin film is chemically stable and soft and does not have negative real component of complex dielectric constant in the whole visible region. Surface plasmon and surface plasmon polariton have potentialities of the development in extremely localized and long-range propagation transmission medium for near future-interconnection system between the integrated electronic circuit and the optical communication circuit. In the actual electronic circuits in Ultra Large-Scale Integration (ULSIs), there is no device and waveguide based on silver but few tens of nanometer copper wirings only. But in CMOS devices, there are TiN thin layers as a copper diffusion barrier, and this film may act as excitation source and waveguide of plasmon or plasmon polariton waves when it has good crystallinity. TiN film is convenient for future optoelectronic circuits because of its compatibility with device fabrication process [1–11].

Titanium nitride (TiN) is one of the multirole compounds used in many technological areas. The application of TiN, which belongs to the early transition metal nitrides, is originated from their decent properties. Namely, they have high electrical and thermal conductivities, which are comparable to metals. Additionally, they are very hard with high melting points. Due to its good corrosion and wear resistances, TiN is used as a protective coating on industrial tools worked in inhospitable environment. With TiN coatings of about 2–10 μm thicknesses tool life is increased several fold generally. TiN also has important tasks in the semiconductor industry. It is used as a diffusion barrier layer in contact structures, both to prevent Cu and to provide an adhesive layer between dielectric

http://dx.doi.org/10.5772/67765

material and Cu. Even though TiN is stable over a broad composition range, its structure and properties depend critically on its actual composition. Electrical resistivity of TiN depends strongly on its stoichiometry and morphology. The presence of oxygen and/or carbon in TiN takes on low hardness and high resistivity. One of the effective compounds is titanium oxynitride (TiON).

In recent research on alternative novel plasmonic materials, silicon, germanium, group III–V nitride semiconductors, arsenides, phosphides, and transparent conducive films are examined energetically. Transition metal nitrides, i.e., TiN, TaN, ZrN, HfN, attract increasing attention because of their golden luster, metallic properties in the Vis-NIR region, characteristics as nonstoichiometric and interstitial compound, and high free carrier densities.

As a result, the optical properties will be controlled by altering the composition of them. These materials are used as a diffusion barrier in damascene interconnect structure and gate metal in p-type/n-type transistor devices. In this work, I have been interested in TiN lately. One of the latest review papers described that this film has been formed widely and intensively by various techniques such as magnetron sputtering, cathode arc discharge, chemical vapor deposition, atomic layer deposition, pulsed laser deposition, ion beam-assisted deposition, high power impulse magnetron sputtering, etc. Achievements of the predecessors gave us various resultant TiN films with many different characteristics, which were quite sensitive to the experimental conditions.

Origin of the studies in disarray may connect closely with chemical composition of the films such as Ti_xN or TiN_x ($x \neq 1$). Also, when the chemical composition is nearly TiN_x ($x \sim 1$), its crystallinity was not enough or crystal grain size was very small. As a result, without taking our eyes off of plasmonics with TiN film, creation of extreme flat TiN film with high crystallinity has been a long-time consuming. Previous studies usually made a reaction field, which contains both Ti and N atoms, and the field was excited by a certain type of electrical discharge or laser-produced plasma. The resultant TiN film was deposited slowly [12–17].

In this study, pulsed laser deposition (PLD) by irradiation of ultraviolet laser pulses has been adopted into the thin-film formation. The reason is because (1) it is a clean process composed of pure solid target, clean substrate, and dense ultraviolet photons only, (2) it may be possible to form a film having a similar chemical composition, and (3) the deposited film thickness can be controlled with laser pulse number basically. In contrast to predecessors in thin film generation of TiN, PLD procedure in this experiment uses a hot pressed target of TiN crystal powder to create a highly crystalline TiN thin film, which is never formed [18–23].

Purposes of this study are (1) clarification of TiN film formation by PLD with the hot pressed TiN target, (2) promising samples culled from the PLD process will be used for basic experiments of surface plasmon resonance excitation, (3) metal-insulator-metal structure will be formed with the TiN film and the AlN film, which will be also deposited by the PLD method, and surface plasmon polarities will be excited in the multilayered structure.

2. First experience with commercial TiN films and instruments for fabrication and analyses of PLDed TiN thin film

At the beginning, since the author has no experience in generating and treating TiN film, several types of TiN samples for comparison were provided by courtesy of Mr. Akitaka Kashihara (Shinko Seiki). The samples were made by RF sputtering based on Ar/N_2 plasma, Ti target, and substrate (GS: S2112 glass slide, Matsunami Glass). Three samples of (a) TiN (50 nm)/GS, (b) SiO_2 (150 nm)/TiN (50 nm)/GS, and (c) TiN (200 nm)/SiO_2 (150 nm)/TiN (50 nm)/GS were produced experimentally with a view to asymmetric MIM structures. The thickness or duration of sputtering was calibrated with other samples.

And (d) a disparate TiN(50 nm)/QZ (Quartz) sample was also given by courtesy of Mr. Kaoru Hoshino (Parker S·N Kogyo). A quartz substrate covered with vacuum evaporated Ti thin film (50 nm) was treated by nitriding process with high temperature nitrogen gas (800°C, 1 hour), which is commonly applied to protection coating of industrial tools.

The X-ray diffraction (XRD) of these thin films was carried out using a Rigaku diffractometer (SmartLab) with a Cu Kα radiation operating at 20 kV voltage and 10 mA current. Unfortunately, most of them did not give effective XRD data. Only sample (c) had sharp three peaks corresponding to TiN(111), (200), and (222), which may be signals from outermost TiN (200 nm) layer and agreed well with previous papers. The thick TiN layer had luster of gold.

XRD data given by Mr. Hoshino showed that a thicker sample, which is the same as sample (d), has sharp peak of Ti_2N. Therefore, high temperature nitriding is good for tool protection but is not good for creation of plasmonic thin film.

As described herein below, samples (a)–(c) did not show good results in X-ray photoelectron spectroscopy (XPS). Therefore, the author chose the PLD method as a film deposition process for plasmonic TiN film. There is a commonly held view that PLD can deposit epitaxial thin film with stoichiometric composition in a clean atmosphere.

Deposition of TiN film was performed using a pulsed third harmonic (3ω) YAG laser system (λ = 355 nm, E_L = up to 350 mJ/pulse, pulse duration τ_L = 3.3 nsFWHM, Powerlite 9010, Continuum) as shown in **Figure 1(a)**. The pulse energy was monitored by a thermopile detector (30A-P-SH (AN/2), Ophir), and the pulse duration was observed by an universal streak camera (C5680-01, Hamamatsu Photonics) (**Figure 1(b)** and **(c)**) coupled with a cooled back-illuminated CCD camera (PIXIS1024B, Princeton Instruments) (**Figure 1(d)**). While most pulsed lasers used for PLD do not pay attention to their temporal pulse shape, and the shape is always considered a smoothed Gaussian, is not it? Actually, they are spiky, and the temporal shape changes with respect to each pulse. Therefore, the author decided to use an injection seeding by extremely narrow-spectrum (<5 kHz) IR fiber laser seeder (SI-2000, NP Photonics) at 1064 nm, and the resultant every pulse shape is maintained in smoothed Gaussian as shown in later. The resultant bandwidth of 3ω pulse was around 0.003 cm^{-1} and also each pulse energy kept constant. This may have the effect of both debris suppression and good surface flatness in the PLD process.

The pulsed laser beam was focused on the PLD target placed in center of the UHV chamber evacuated to 5×10^{-5} Pa by turbo-molecular pump (TMP, Varian) coupled with a dry scroll vacuum pump

http://dx.doi.org/10.5772/67765

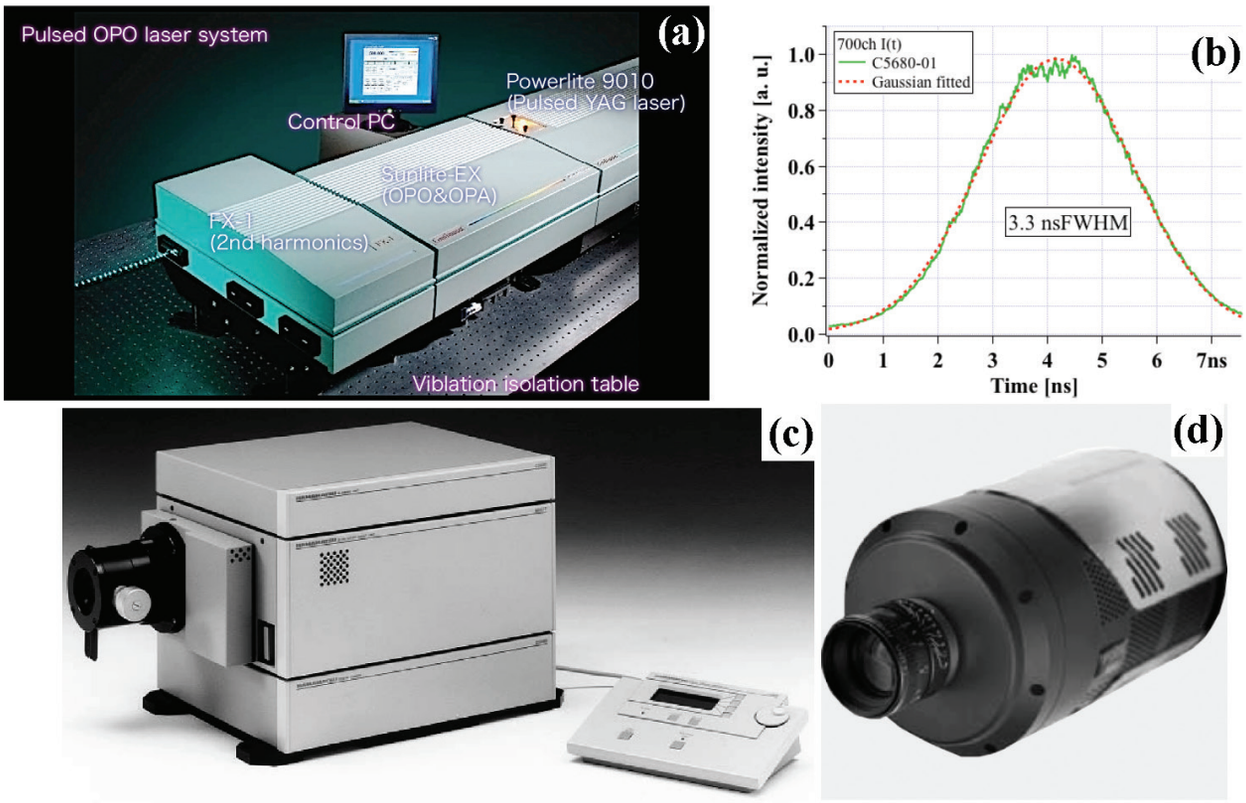

Figure 1. (a) An injection-seeded pulsed YAG laser (powerlite precision 9010) with OPO/OPA and doubler system (sunlite-EX & FX-1). (b) Typical temporal intensity profile of 355-nm pulse recorded by a streak camera. (c) A universal streak camera (C5680-01) and (d) a back-illuminated cooled CCD camera (PIXIS 1024B).

(SP, ANEST IWATA) as shown in **Figure 2**. The stoichiometric hot pressed TiN target (φ = 20 mm, t = 5 mm, three nines purity, filling rate = 88.6%, mass density = 4.65 g/cc, Toshima Manufacturing) was ablated at a pulse intensity ranging from 5.8×10^8 to 1.4×10^{10} W/cm^2 with pulse repetition rate of 10 Hz for several tens of minutes. For near future experiment for insulator film, a hot pressed AlN target (φ = 20 mm, t = 5 mm, three nines purity, filling rate = 99.4%, mass density = 3.24 g/cc, Toshima Manufacturing) was also prepared.

The glass substrate, kept around 5 cm away from the target without thermal control, was set through load lock chamber (TMP-pumped), which is positioned at right angle with laser optical axis, and temperature of target and substrate went along with the situation.

The PLD target hangs down from a vertically installed vacuum attachment rod, and the vertical position was set by a rack and pinion adjustment (±10 cm). The surface of PLD target makes a 360-degree turn by the rod. As a result, any position of the target was shot at any angle of incidence (typically 60°), and multilayer coating is available without exposure to the atmosphere when several different targets are installed. The deposition was carried out in the PLD chamber without introduction of nitrogen gas, and the chamber pressures were ranging from 10^{-4} to 5×10^{-4} Pa during deposition.

The 3ω laser pulse, which plane of polarization was adjusted to the vertical direction by a half-wave plate, was gradually focused via a AR-coated quartz plane-convex lens (f = 750 or 500 mm)

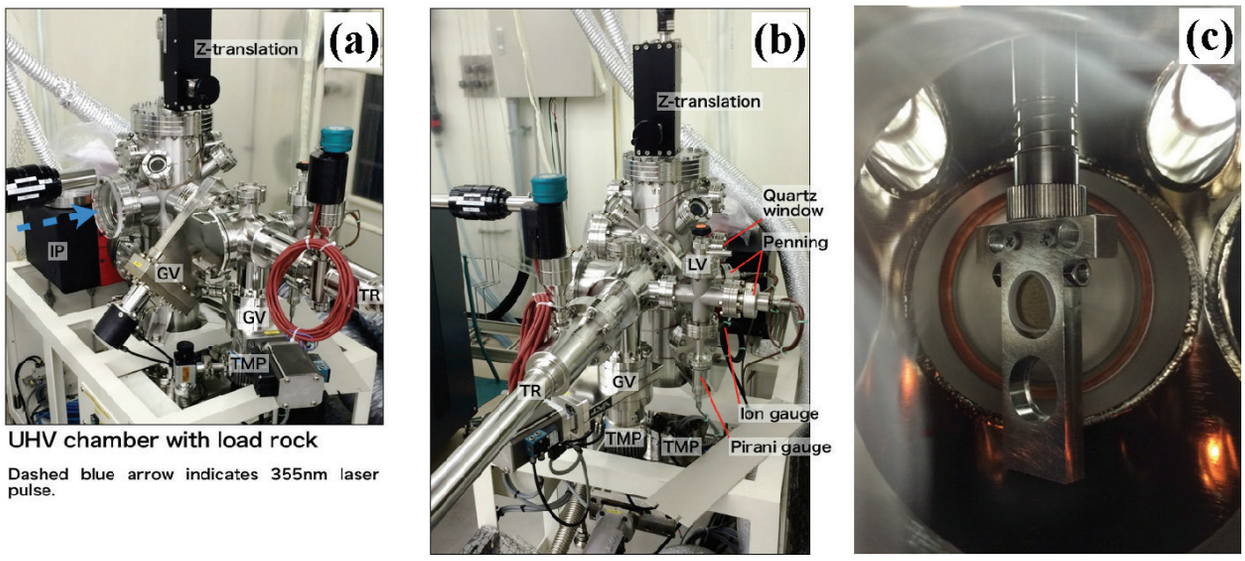

Figure 2. (a)(b) A UHV vacuum chamber system used in PLD experiments. (c) A photo of hot pressed TiN target installed in the center of UHV chamber.

struck the target surface through a homebuilt quartz Brewster window (θ_{inc} = 56°, t = 5 mm), as shown in **Figure 3**.

The deposition rate of the TiN films was investigated by measuring a height of artificially produced sub-wavelength step w/ and w/o mask during the PLD process. The step height was observed by both an optical surface profiler (NewView, Zygo) and a surface texture and contour measuring instruments (SURFCOM 1400D, Tokyo Seimitsu) as shown in **Figure 4(a)** and **(b)**, and it was determined to be close to 50 nm for a deposition period of 5 min with pulse energy of 340 mJ on target.

The substrate used in the PLD process was a glass slide as mentioned above and was cleaned by ultrasonic bath in the order of acetone, ethanol, and ultrapure water for 10 min each.

As a guide, time-integrated emission spectrum of the PLD plume ranging from 350 to 1050 nm was recorded by a diffraction grating spectrometer (USB4000, Ocean Optics) (**Figure 4(c)**) through a multimode optical fiber, in which one end faced to the chamber center. Scattered 3ω light was strongly attenuated by a UV-cut filter (MC UV SL-39, Kenko Tokina) for SLR cameras. Spectrometer wavelength calibration was carried out with 2ω (λ = 532 nm) and 3ω (λ = 355 nm) laser pulses, helium-neon laser (λ = 632.8 nm, Melles Griot), multiline argon ion laser (488 and 514.5 nm, Edmund Optics) and its argon lines (650–850 nm) from the discharge.

Spectral reflectance of the deposited TiN film was measured by an UV-Vis/NIR spectrophotometer (U-4000, Hitachi High-Technologies) (**Figure 5(a)**). Using a specified optional attachment, five-degree absolute and unpolarized specular reflectance of the sample were observed. A field of the measurement was 5 × 10 mm^2.

A one-time measurement for estimation of spectroscopic complex refractive index at the visible region was carried out by a spectroscopic ellipsometer (GES5E, SOPRA) with TiN film (50 nm) as shown in **Figure 5(b)**.

http://dx.doi.org/10.5772/67765

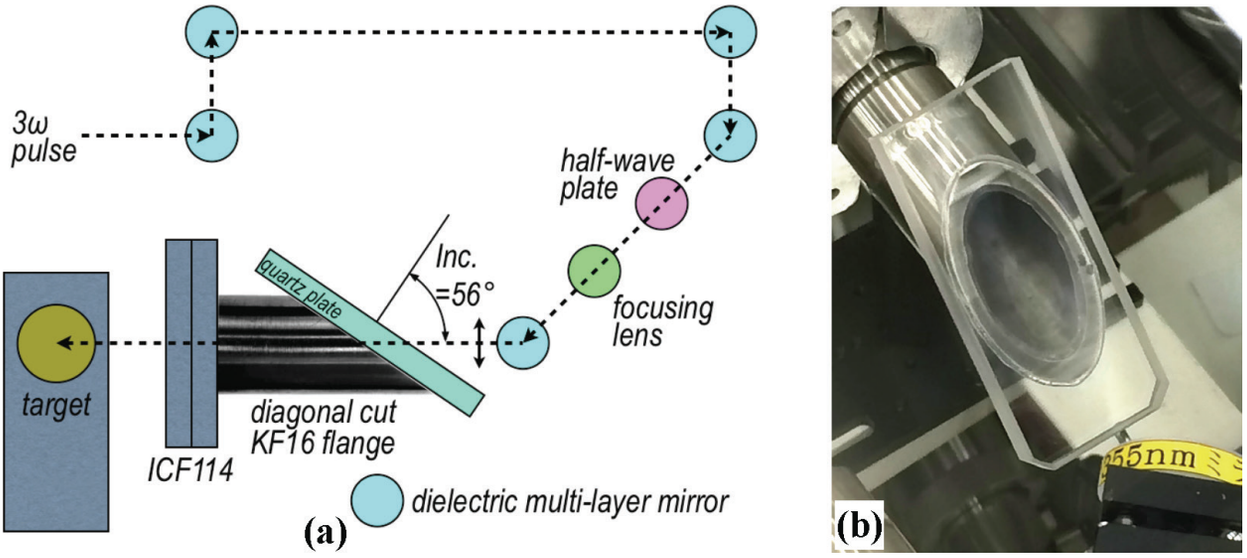

Figure 3. (a) Schematic diagram of optics used for guiding 3ω pulse into the UHV chamber center. (b) A photo of self-produced quartz Brewster window, which is effective with a half-wave plate.

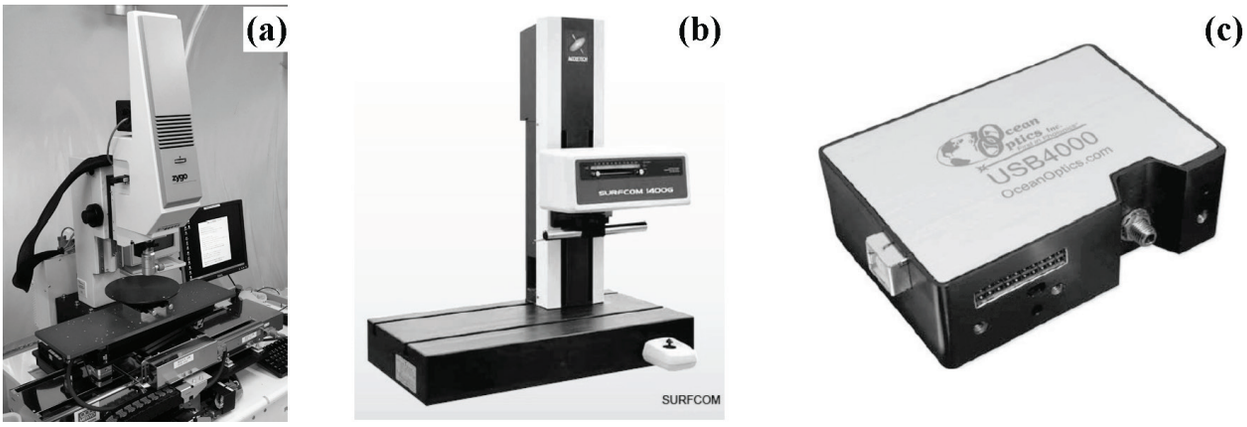

Figure 4. (a) An optical surface profiler by white-light interferometry (NewView). (b) A surface texture and contour measuring instrument (SURFCOM 1400D). (c) A fiber-type diffraction grating spectrometer (USB4000).

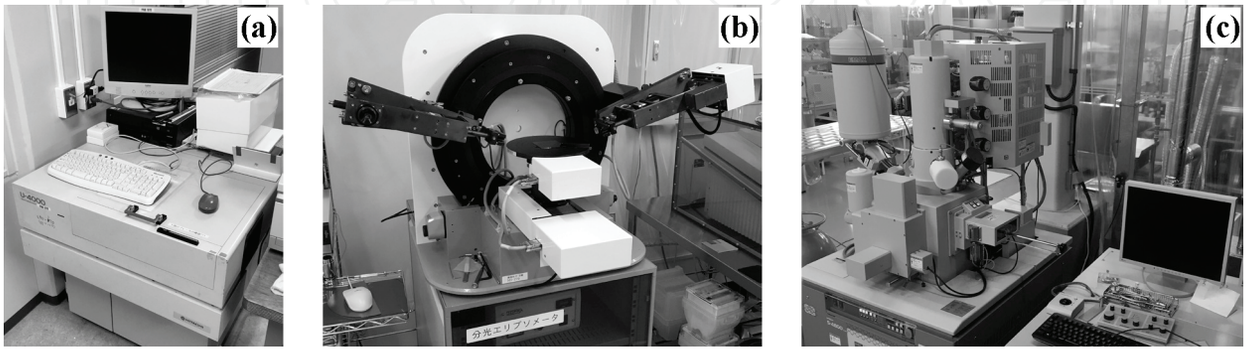

Figure 5. (a) A UV/Vis-NIR spectrophotometer (U-4000). (b) A spectroscopic ellipsometer (GES5E). (c) A scanning electron microscope (S-4800).

Position-dependent appearance, surface flatness, and existence of micro- and nanoparticles or debris were studied by a scanning electron microscope (SEM) (S-4800, Hitachi High-Technologies) (**Figure 5(c)**). Also, examinations of both a filling factor and growth process were performed with the SEM images.

Crystallinity of the PLD target was characterized by an X-ray diffractometer (XRD) (SmartLab, Rigaku) (**Figure 6(a)**) with Cu-Kα line (λ = 0.154 nm, E = 8.05 keV) before use. In this chapter, all the XRD patterns shown were measured by 2θ-ω scan with a crystal monochromator (Ge(220)×2). **Figure 13(a)** shows the XRD patterns of polycrystalline TiN. The diffraction peaks located at 2θ = 33.7°, 42.6, 61.8, 74.1 and 78.0° are corresponding to (111), (200), (220), (311), (222) of TiN, respectively. These peaks confirm that the PLD target is hot pressed polycrystalline TiN. But, an extra peak was found unexpectedly at 2θ = 25°, and this may be correspond to (101) of anatase-type titanium dioxide because the base powder may contain traces of oxygen. Deposition of TiN will be done with this target at the moment.

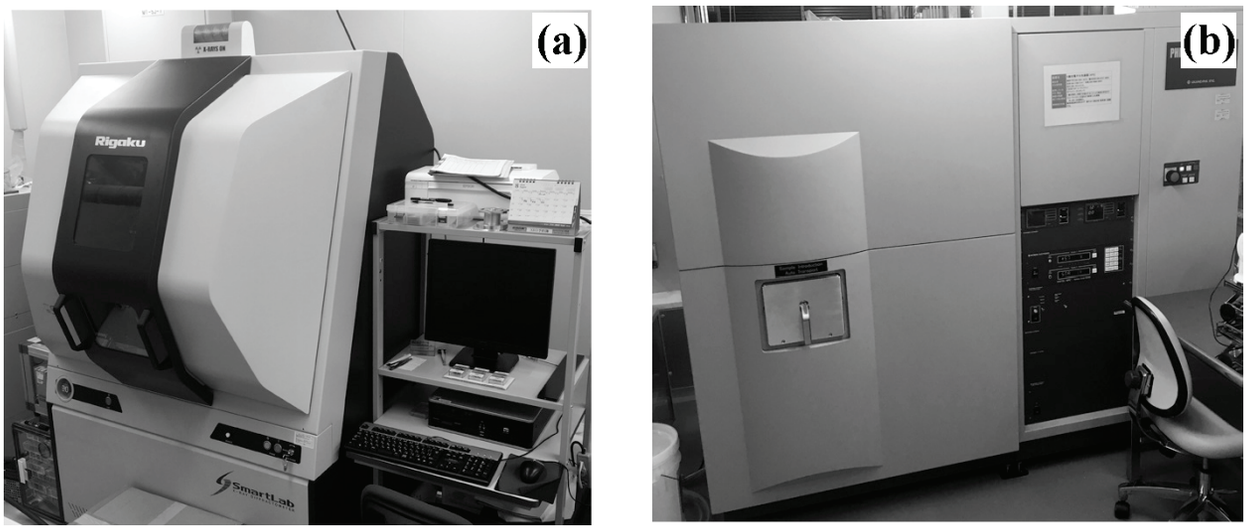

Figure 6. (a) X-ray diffractometer (SmartLab). (b) X-ray photoelectron spectroscopy system (PHI quantum2000 scanning ESCA microprobe).

Elemental composition, empirical formula, chemical state, and electronic state of the elements that exist within the TiN film was analyzed by a monochromatic X-ray photoelectron spectroscopy (XPS) system (PHI Quantum 2000 Scanning ESCA Microprobe, ULVAC-PHI) with Al Kα line (λ = 0.834 nm, E = 1.487 keV) as shown in **Figure 6(b)**.

3. Experimental results

3.1. Outline of the PLD experiment

Experimental condition is summarized in **Table 1**. The 3ω laser pulse is gradually focused by AR-coated flat-convex lens, and lens-target distance is adjusted to realize moderate intensity for laser irradiation. Basically, laser pulse energy is adjusted to maximum output.

http://dx.doi.org/10.5772/67765

Sample No.	focal length (flat-convex lens)[mm], coating	lens - target distance [mm]	E_{p_YAGout} [mJ/pulse] (3.3nsFWHM)	No. of 3ω mirror, R_{total}	No. of lens, T_{total}	terget - glass distance [mm]	No. of Brewster window, T_{total}, λ/2-plate	θ_{inc} of laser [deg]	PLD duration [sec], E_{total}[J]	Vacuum during PLD [Pa]	I_{Lave}[W/cm²], spot area [mm²], E_T[J/cm²/pulse]	outcome, appearance, analysis
1(⑤)	750 AR	415	360 (347.4 on T)	5 0.9995	1 0.98	50	1 0.99	60	600 2084.4	4.5E-4	5.26E+8 20 1.737	△ frosted
2(⑥)	750 AR	415	360 (347.4 on T)	5 0.9995	1 0.98	50	1 0.99	60	1200 4168.8	4.5E-4	5.26E+8 20 1.737	△ frosted
3(⑦)	750 AR	615	360 (347.4 on T)	5 0.9995	1 0.98	50	1 0.99	60	600 2084.4	4.5E-4	3.23E+9 3.26 10.656	◎ mirrored XPS
4(⑧)	750 AR	615	360 (347.4 on T)	5 0.9995	1 0.98	50	1 0.99	60	1200 4168.8	4.5E-4	3.23E+9 3.26 10.656	◎ mirrored XRD,XPS
5(⑨)	750 AR	515	360 (347.4 on T)	5 0.9995	1 0.98	50	1 0.99	60	1200 4168.8	4.5E-4	7.63E+8 9.82 3.538	△ frosted flake off
6(⑩)	750 AR	575	360 (347.4 on T)	5 0.9995	1 0.98	50	1 0.99	60	600 2084.4	4.5E-4	1.92E+9 5.48 6.34	◎ mirrored XRD,XPS
7(⑪)	750 AR	655	360 (347.4 on T)	5 0.9995	1 0.98	50	1 0.99	60	300+600 3126.6	4.5E-4	6.53E+9 1.612 21.55	mirrored step (50 nm)
8(⑫)	500 AR	455	360 (340 on T)	5 0.9995	1 0.98	70	1 0.99 #	60	2400 8160	4.5E-4	1.27E+10 0.814 41.77	◎ mirrored XPS
9(⑬)	500 AR	455	360 (340 on T)	5 0.9995	1 0.98	70	1 0.99 #	70	2400 8160	4.5E-4	8.66E+9 1.190 28.57	◎ mirrored XPS

 # half-waveplate(T=97.875%) was added for fine adjustment of polarization of laser pulse, and the resultant edge reflection of the Brewster window decreased.
⑤～⑬: serial number of the sample since the beginning of PLD experiment.

Table 1. Summary of the PLD experiment for the TiN thin film. Basically, double circles marked in rightmost column show acceptable results.

The plume flux ablated from the PLD target is so strong, and target-substrate distance is set more than 50 mm to suppress both sputtering and clacking of the deposited thin film. Incident angle of the laser pulse is set at 60° because a glass substrate is set at 90° from optical path of the laser beam. Duration of the PLD process is determined for thin film fabrication. Although base pressure of the main vacuum chamber is lower than 10^{-4} Pa, the load-lock system is used as a holder of a glass substrate, and the main and sub-chambers are connected. Then the PLD process is performed in a vacuum of 4.5×10^{-4} Pa. Laser irradiation intensity is adjusted by changing lens-target distance, and is realized from 5×10^{8} to 10^{10} W/cm^2. Rightmost column in Table 1 describes visual of the resultant film and X-ray analysis worked. In **Figure 7**, photos of well-deposited TiN films are shown, and adhesion of these films is quite good.

3.2. Reflectance spectrophotometry (U-4000)

By using a U-4000 spectrophotometer, unpolarized spectral reflectance at 5 degree was measured. As the digital photo shows, a mirrored PLD film of TiN had metallic cluster-like gold film, and the spectral reflectance appears to be the same as gold. Typical spectra reflectance curves are shown in **Figure 8**.

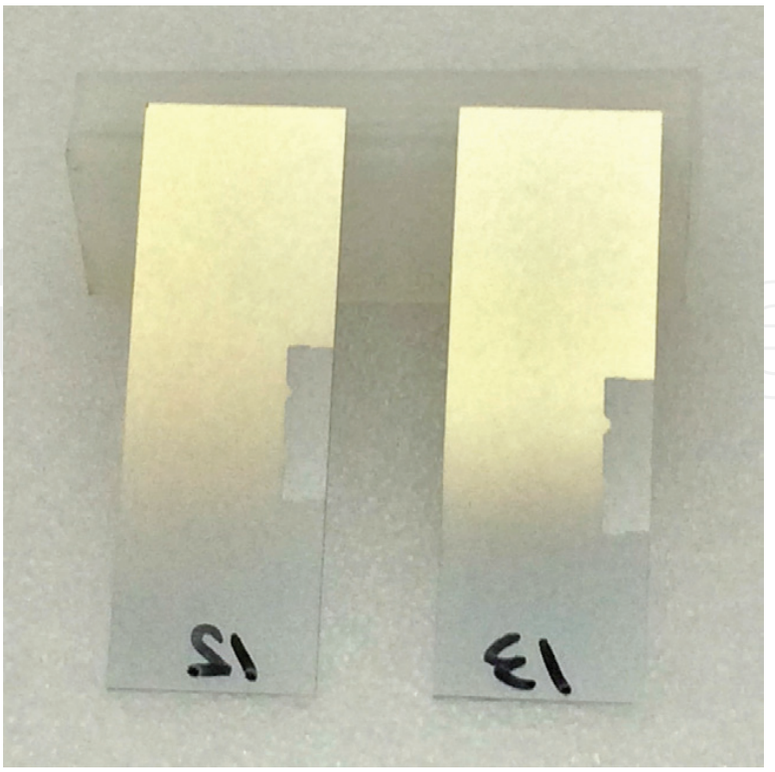

Figure 7. Photo of the PLDed TiN thin film (sample ⑫ & ⑬ in **Table 1**) on a glass slide.

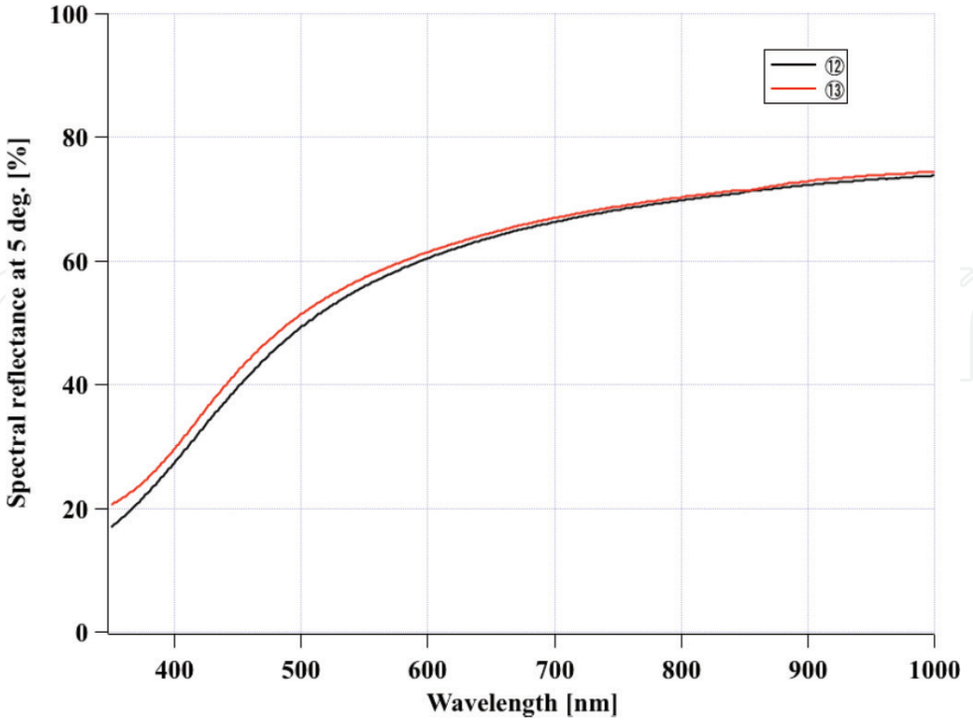

Figure 8. Unpolarized spectral reflectance of the PLDed TiN thin film (⑫ & ⑬ listed in **Table 1**).

http://dx.doi.org/10.5772/67765

3.3. Spectroscopic ellipsometry (GES5E)

Because of the instrument failure, spectroscopic ellipsometry for the TiN film was done only once before. Refer to the built-in database of refractive index, 50-nm-TiN film on a glass slide was measured by SE. Both the film thickness and the spectral complex refractive index were determined by the method of least squares. The resultant film thickness is almost same as 50 nm, and dependence of the index on light wavelength is also coincident with the database (**Figure 9**) [24–29].

3.4. Optical emission spectroscopy (USB4000)

Time-integrated optical emission spectrum of the PLD atmosphere or blight plume was measured by a fiber-type USB4000 grating spectrometer with a recorded wavelength range of 350–1000 nm, as shown in **Figure 10**. The input multimode optical fiber end was set at the right angle to one of the glass (Kovar) viewports installed on the experimental chamber. Through the viewport, light emission of the plume was collected at 45° from the PLD target normal.

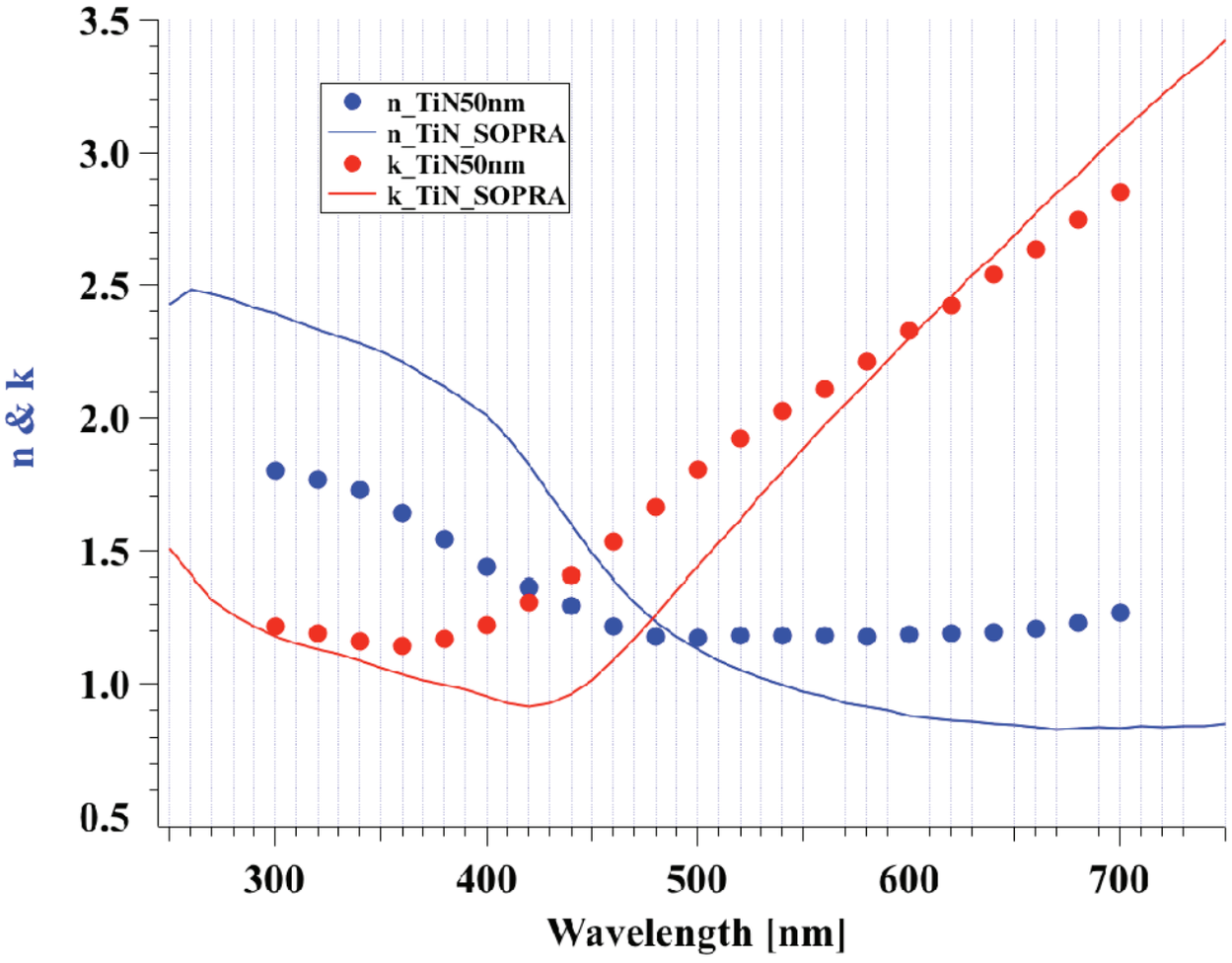

Figure 9. Complex refractive index curve of the PLDed TiN thin film determined by SE. Solid lines indicate a built-in reference data of TiN.

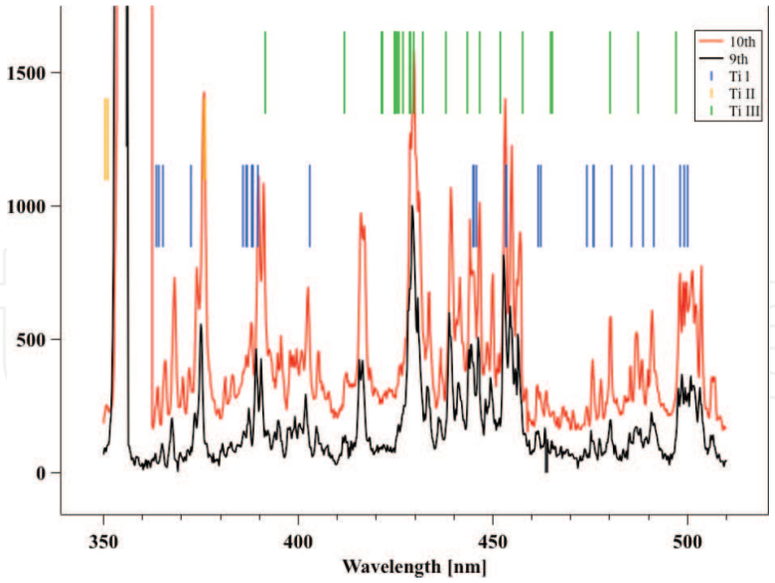

Figure 10. Time-integrated optical emission spectra of the samples ⑨ & ⑩ listed in **Table 1**. Colored markers of short line indicate line positions of both Ti atoms and Ti ions.

Because of low irradiation intensity of the pulsed UV laser light and non-use of discharges, neither multicharged titanium ion nor band emission of nitrogen was observed. In the UV region, emission of both Ti atom and singly ionized Ti atom was recorded.

3.5. White-light interferometry and stylus profilometry (NewView and Surfcom)

Estimation of a mean deposition rate of the PLD process was carried out by making a step on a film surface. After deposition of thin TiN layer, a part of the surface was masked, and additional deposition of TiN layer was executed for 5 min. The height of the handmade step was determined to be about 50 nm by a NewView interferometer, as shown in **Figure 11(a)**. Therefore, the mean deposition rate was estimated to be about 10 nm/min, and the PLD system will be able to control thickness of the film down to the sub-nanometer. The same step structure was also scanned by Surfcom, and the resultant height was same as that of NewView (**Figure 11(b)**).

3.6. Scanning electron microscopy (S-4800)

The surface of TiN thin film was observed by a scanning electron microscope as shown in **Figure 12**. Both (1) degradation of surface flatness of the film caused by shower of micro-nano debris presented in the PLD plume and (2) mass generation of Surface Plasmon Polariton (SPP) scatterer caused by buried debris become major problems in usual PLD process. At the beginning of this study, a glass slide was set within striking distance from the PLD target, and the resultant TiN film was powerfully influenced by spatial distribution of the PLD plume. Therefore, an extensive range of the film was observed by SEM, and the cross-sectional surface of peeling film was examined at high spatial resolution to find internal structure of the PLDed film. Then the central region of the film surface irradiated by very intense and hot

http://dx.doi.org/10.5772/67765

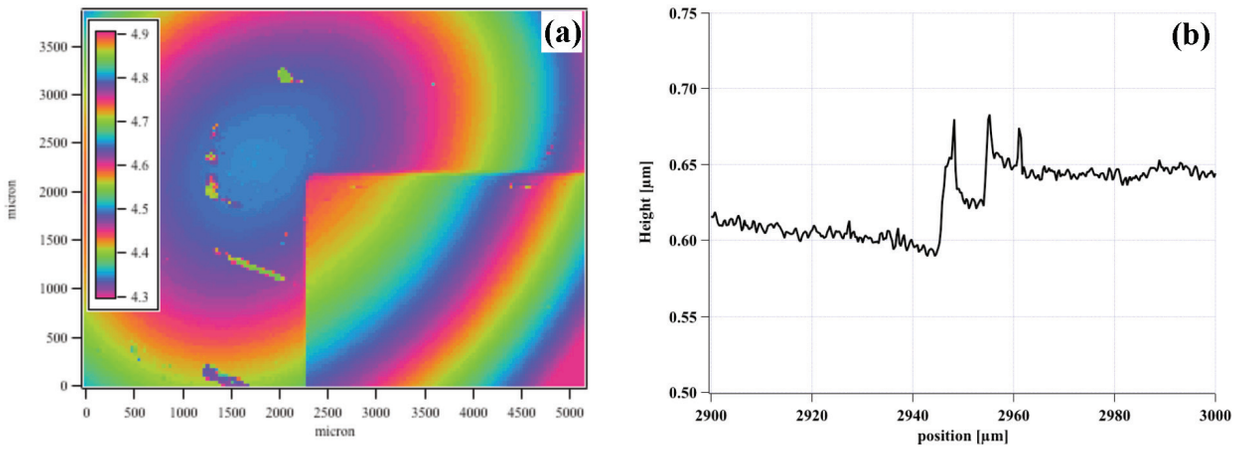

Figure 11. (a) Colored contour image, which was recorded by NewView, of the surface of PLDed sample (⑪ listed in **Table 1**) fabricated by two consecutive PLD processes. Square area (lower right) was masked during the second PLD process. Hence, the height is lower than that of upper left area. (b) Cross-sectional curve across the step structure recorded by Surfcom. Small dip at 2950 μm is no more than an unexpected hole.

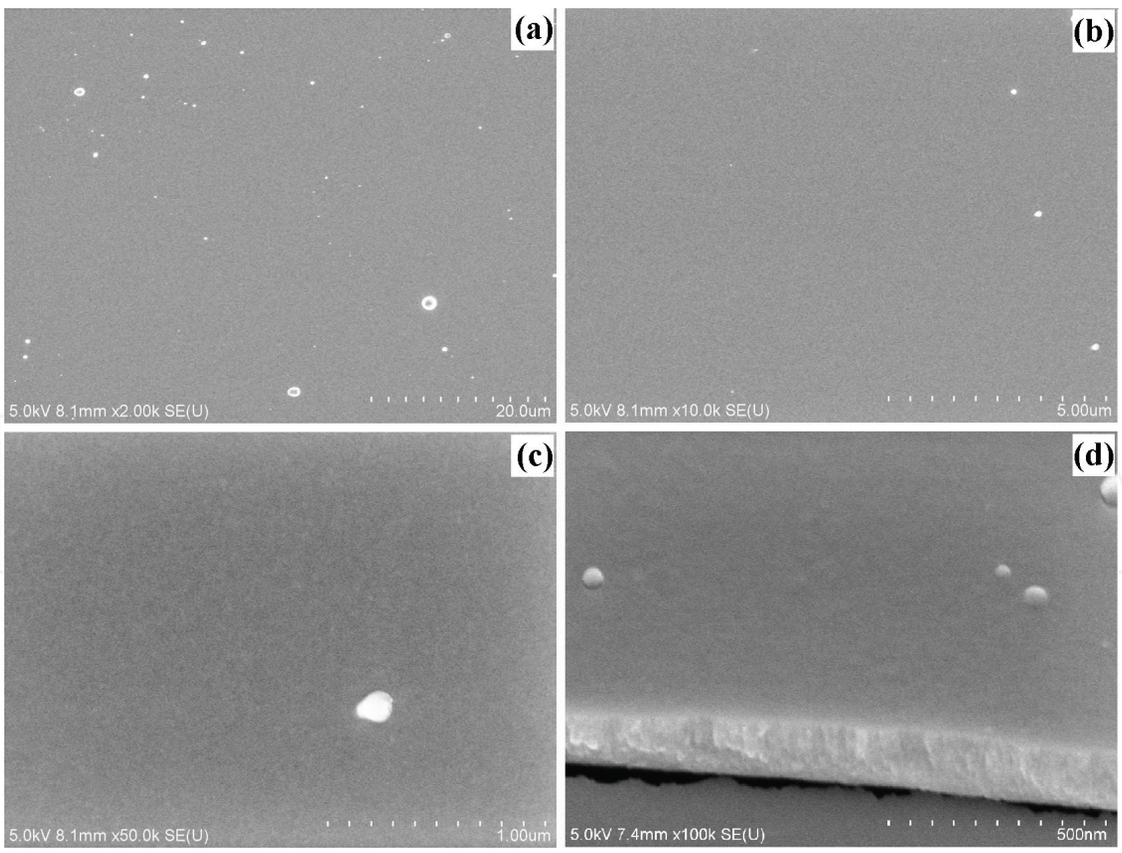

Figure 12. (a)–(c) SEM images of the PLDed TiN thin film (⑩ listed in **Table 1**). Debris is observed sparsely. (d) Cross-sectional SEM image of the PLDed thin film taken by oblique observation. Dense and flat structure of the film are observed clearly.

plume tarnished and cracked, and small pieces of peeling film existed. In the meantime, the film created by irradiation of fringe region of the plume had mirror completion, and the surface flatness was acceptable without dense flux of debris. Cross section of the peeling film was observed at maximum useful magnification (up to 100k), and an interior of the film seemed to be well filled without any apparent void. The cross-sectional surface had snaky and streaky structure in a longitudinal (surface normal) direction, and the growth of thin film may be governed by (111)-oriented growth. For this reason, out-of-plane XRD pattern of the film had a (111) peak only and in-plane pattern had no peaks.

3.7. X-ray diffractometry (SmartLab)

Application of TiN film for plasmonic phenomena is coupled with high crystallinity and large grain size in the film, and I decided to think a great deal about film quality before impending goal, i.e., excitation of SPP with TiN film. Crystallinity of the PLDed TiN film was examined by an X-ray diffractometer with a 2θ-ω scan (out-of-plane) method [30–32]. The PLD target was a hot pressed pellet of microcrystalline TiN powder and showed all the major peaks listed in well-known XRD databases as shown in blue curve of **Figure 13(a)**. Then TiN film, which was fabricated on a glass slide by plasma-assisted sputtering, was analyzed and only a weak (111) peak was observed. On the other hand, TiN film on a silicon (100) surface, which was fabricated by the same process, had no peak of TiN but Si(400) only, as shown in grey curve of **Figure 13(a)**. The PLDed TiN film had (111) and (200) peaks and had no peak in in-plane scan, as shown in **Figure 13(b)**. Therefore, highly (111)-oriented growth may act in a dominate fashion in the PLDed TiN film on a glass slide.

3.8. X-ray photoelectron spectroscopy (Quantum 2000)

Previous reports regarding TiN thin film fabrication, one of the major issues is an unexpected chemical composition of TiN and unwanted compound incorporation in the film. That is why

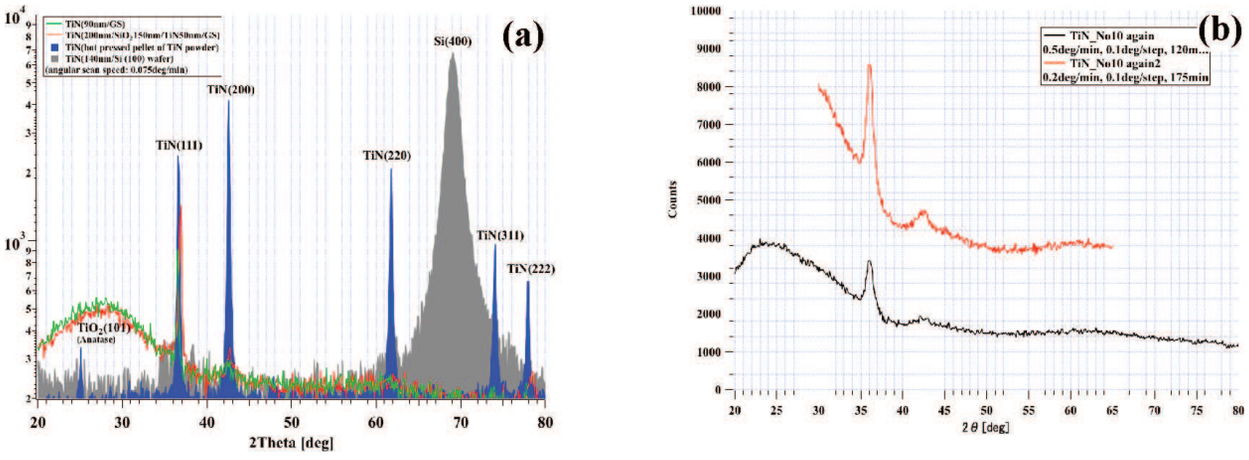

Figure 13. (a) XRD patterns of hot pressed PLD target and TiN film fabricated by plasma-assisted sputtering. (b) XRD pattern of the PLDed TiN thin film (⑩ listed in **Table 1**). The PLDed film is (111)-oriented, and the thickness is not enough to show higher order peaks.

http://dx.doi.org/10.5772/67765

an X-ray photoelectron spectroscopy was applied to the surface of TiN films fabricated by both plasma-assisted sputtering and PLD [33–38]. Every XPS analysis was carried out with X-ray beam at the right angle to the film surface. The survey spectrum was recorded in a binding energy of −8 to 1398 eV at low resolution (ΔE = 1 eV), and high-resolution photoelectron spectra were measured for estimation of N(1s), O(1s), Ti(2s), and Ti(2p) as relevant atoms (ΔE = 0.05 eV) as shown in **Figures 14** and **15**. Additionally, C(1s) was diagnosed for estimation of surface contamination and absolute energy reference for chemical shifts. The measurement took about 1 hour for each atom. All the XPS spectra were measured clearly, and the principal difference between the two films is noticeable on the spectrum of Ti(2p). The Ti(2p) spectrum has more peaks, which are strongly associated with a valuable work of Jaeger et al. [33]. Namely, peaks of Ti $2p^{3/2}$ and shake-up$^{3/2}$ are observed clearly. In the N(1s) spectrum, a peak originated from the N-Ti bond is much stronger than that of the O-Ti bond. In the O(1s) spectrum, a peak of the O-Ti bond is stronger than that of the O-N bond. The Ti(2s) spectrum is also obtained clearly with the PLDed film, and

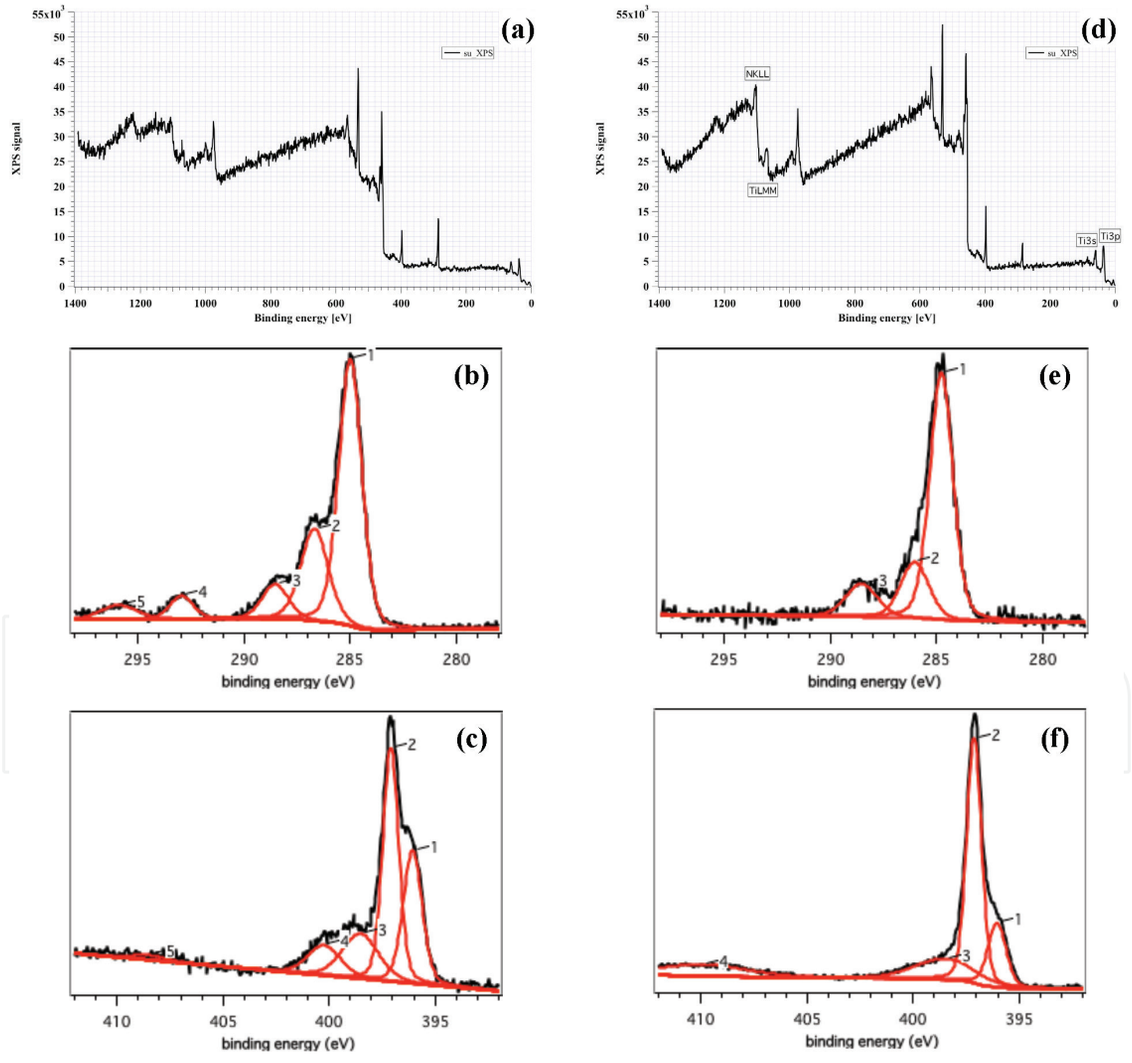

Figure 14. (a) Survey, (b) C(1s), (c) N(1s) spectrum of the sputtered TiN thin film recorded by XPS. (d) Survey, (e) C(1s), (f) N(1s) spectra of the PLDed TiN film (⑩ listed in **Table 1**). Gray Gaussian curves are results of peak fitting by Igor Pro coupled with XPST 1.1 [39].

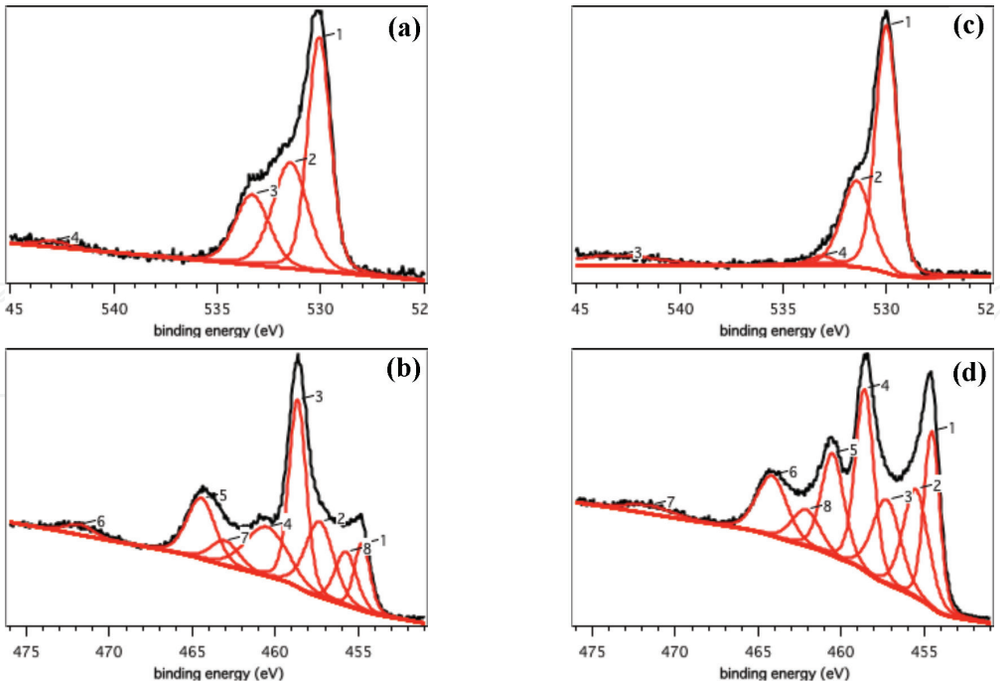

Figure 15. XPS spectrum of the sputtered TiN thin film (a) O(1s), (b) Ti(2p). XPS spectrum of the PLDed TiN thin film (⑩ listed in **Table 1**) (c) O(1s), (d) Ti(2p). In (d), two peaks originate from Ti-N combination are clearly observed, and the same two peaks do not exist in (b). Therefore, the PLDed TiN film may contain much Ti-N combinations.

broadened peak of first-order surface plasmon is also indicated. The high-resolution XPS spectra of N, O, and Ti are indicated simultaneously in **Figure 16** with peak positions referenced from NIST database. The N(1s) peak data agree well with Ti-N bonding. The O(1s) peak suggests the existence of titanium oxide in the PLDed film surface only. The Ti(2p) peaks seem to be close to peaks originated from the Ti-N bonding, but these are clearly influenced by oxides.

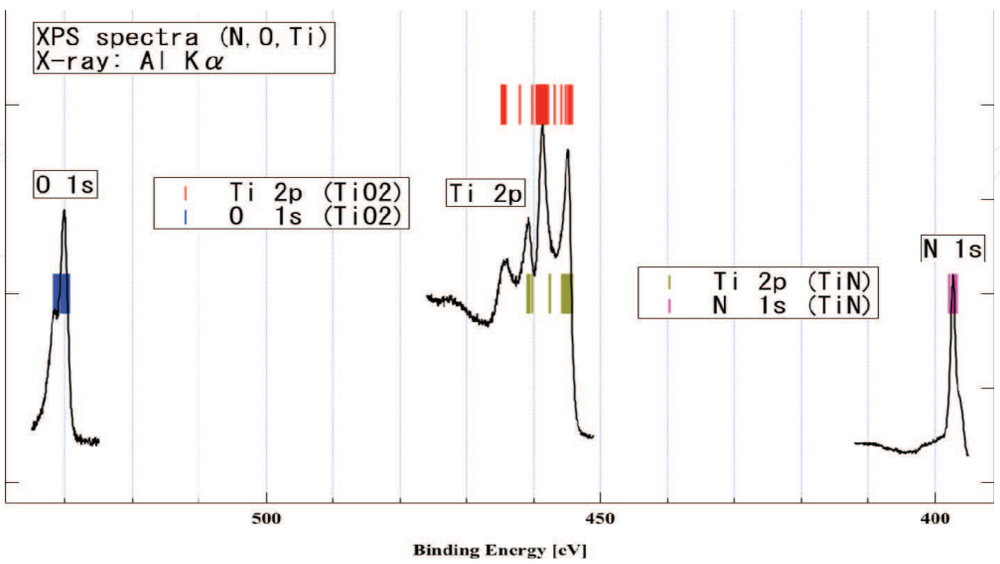

Figure 16. XPS spectra (N, O, Ti) of the PLDed TiN thin film (⑧ listed in **Table 1**) with reference peak positions (colored lines) related to TiN and TiO_2 combinations from the XPS database in the NIST homepage. TiN-based peaks are clearly observed, but TiO_2-based peaks are also exist because there might be considerable residual oxygen in the vacuum used for the PLD process.

http://dx.doi.org/10.5772/67765

4. FEM simulation

It is usually hard to observe excited surface plasmon polaritons in plasmonic experiments. So I have been performed numerical simulation concerning MIM structure with TiN as a metallic layer. A two-dimensional FEM model of MIM structure was designed as TiN(30 nm)/SiO_2(150 nm)/TiN(200 nm) layers on a glass substrate. And the multilayer was irradiated by *p*-polarized light by changing both incident angle and wavelength. As a well-known fact, the MIM structure could excite SPPs inside the insulating layer at small incident angles, and the wavelength of SPPs tends to be larger than the incident wavelength of light. Therefore, the model length in the *x*-direction is set at 2000 nm. The numerical simulation was done by an FEM-based electromagnetic simulation package, COMSOL Multiphysics and WaveOptics Module. In the calculation, the incident angle of light was changed from 0 to 75 degree at 15-degree interval. Increase in the incident angle caused (1) decrease in maximum at 550 nm and (2) blue shift in minimum at 670 nm (dip caused by SPPs) as shown in **Figure 17(a)**. With this result, the incident angle was fixed at 5 degree, and the dependence of minimum on the thickness of thinner TiN layer was simulated. The minimum fell to almost zero at TiN thickness of 20 nm. Calculated E_y map in the MIM structure is shown in **Figure 17(b)**. The incident wave is clearly indicated as a parallel pattern because no reflected wave exists. Inside the insulating layer (SiO_2), we can see intense and confined SPPs having extremely long space wavelength in the *x*-direction. So we could excite SPPs inside the MIM structure with TiN and SiO_2 but we need thinner-than-normal TiN layer for most efficient excitation of the SPPs. On the other hand, the thicker TiN layer must get thicker (>200 nm) to become perfect mirror layer.

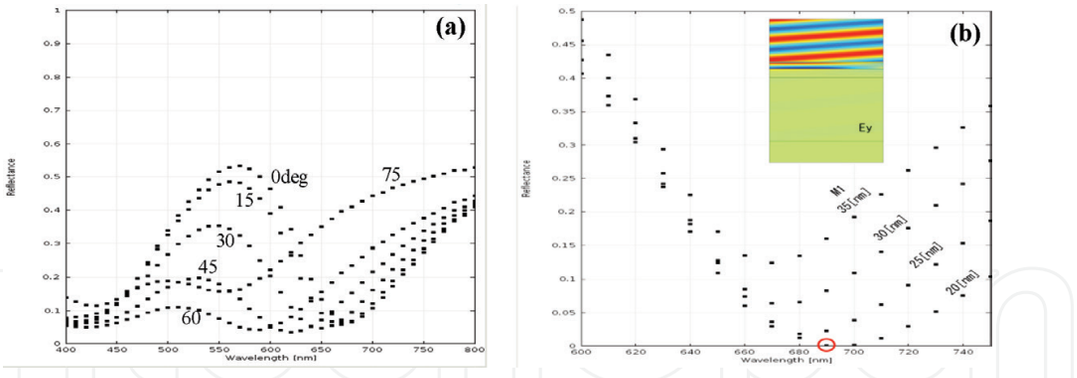

Figure 17. (a) Spectral reflectance curves of asymmetric MIM structure having TiN (30 nm)/SiO_2 (150 nm)/TiN (200 nm) layers on a quartz substrate depend on an incident angle of p-polarized light. (b) Minimum around 680 nm fell to almost zero at TiN thickness of 20 nm. The inset shows electric filed component *Ey* distribution inside the MIM structure. Top-striped area corresponds to vacuum layer just above the thin TiN layer, and most of the incident light converted into plasmon wave inside the MIM structure.

5. Conclusion

Thin film fabrication of titanium nitride has been studied by pulsed laser deposition with third harmonics of Nd:YAG laser. A metallic and adhesive thin film on a glass slide has been deposited at around 10^{10} [W/cm^2] of laser irradiation intensity. The mean deposition rate is

around 10 nm/min. The PLDed TiN film has dense structure and is (111)-oriented by SEM and XRD analysis. Chemical composition analysis of the PLDed TiN film by XPS has good peaks related to Ti and N, but there are considerable influences of residual oxygen because of air-based vacuum. In the near future, a nitrogen-based high vacuum atmosphere will be realized, and XPS peaks of TiO_2 may be suppressed, and basic plasmonic experiments will be performed with the PLDed TiN film coupled with also PLDed AlN film.

Acknowledgements

The author expresses his deepest appreciation for overhaul and repair assistance to the relevant instruments from Center for Scientific Instrument Renovation and Manufacturing Support (CRM), Osaka University. The author also appreciates Dr. Jangwoo Kim (Staff Scientist, Postech) and Dr. Takahiro Yamada (Research Assistant Professor, Osaka University) for helping the XRD operation. The author gratefully acknowledges the technical support of the XPS operation by Mr. Kohei Hosoo (Master's Student, Osaka University) and Dr. Kenta Arima (Associate Professor, Osaka University). The author would like to acknowledge Dr. Katsuyoshi Endo (Professor, Osaka University) for his gratuitous conveyance of his spent- and well-preserved UHV chamber system. Several high power laser optics devices were provided by courtesy of Dr. Tomoyoshi Suenobu (Assistant Professor, Osaka University) and Dr. Mizuho Morita (Professor, Osaka University). Part of fabrication process for self-produced Brewster window was supported by Mr. Tadashi Hayashino (Technical Staff, Osaka University). Numerical electromagnetic simulation by COMSOL Multiphysics was done with technical support from Keisoku Engineering System Co., Ltd. and COMSOL Inc.

Author details

Yasushi Oshikane

Address all correspondence to: oshikane@prec.eng.osaka-u.ac.jp

Department of Precision Science & Technology and Applied Physics, Graduate School of Engineering, Osaka University, Suita, Osaka, Japan

References

[1] S. Rajak et al., Titanium nitrides as plasmonic materials in visible frequency range, Proc. of SPIE, Vol. 9654, 965412 (2015), doi: 10.1117/12.2181622.

[2] A. E. Khalifa et al., Plasmonic silicon solar cells using titanium nitride: a comparative study, J. Nanophotonics, Vol. 8, 084098 (2014).

[3] H. Mekawey et al., Dispersion analysis and engineering in TiN 2D plasmonic waveguides, Proc. of SPIE, Vol. 9371, 93711C (2015), doi: 10.1117/12.2076651.

[4] G. V. Naik et al., Oxides and nitrides as alternative plasmonic materials in the optical range, Opt. Mat. Exp., Vol. 1, No. 6, pp. 1090-1099 (2011).

[5] G. V. Naik et al., Alternative plasmonic materials: beyond gold and silver, Adv. Mat., Vol. 25, No. 24, pp. 3264-3294 (2013).

[6] P. Patsalas et al., Optical properties and plasmonic performance of titanium nitride, Mater., Vol. 8, pp. 3128-3154 (2015), doi:10.3390/ma8063128.

[7] V. Braic et al., The influence of deposition parameters on optical properties of titanium nitride thin films, Proc. of SPIE, Vol. 2461, pp. 597-599 (1995).

[8] N. Kinsey et al., Effective third-order nonlinearities in metallic refractory titanium nitride thin films, Opt Mater Express, Vol. 5, No. 11, pp. 2395-2403 (2015), doi: 10.1364/OME.5.002395.

[9] P. Patsalas et al., Optical, electronic, and transport properties of nanocrystalline titanium nitride thin films, J. Appl. Phys., Vol. 90, No. 9, pp. 4725-4734 (2001).

[10] Y. Zhong et al., Review of mid-infrared plasmonic materials, J. Nanophotonics, Vol. 9, 093791 (2015).

[11] F. Chiadini et al., Composite surface-plasmon-polariton waves guided by a thin metal layer sandwiched between a homogeneous isotropic dielectric material and a periodically multilayered isotropic dielectric material, J. Nanophotonics, Vol. 9, 093060 (2015).

[12] S. Fu et al., Impact of the basal material on the deposition titanium nitride thin films, Proc. of SPIE Vol. 9285, 928507, doi: 10.1117/12.2069017.

[13] S. Fu, The study of substrate material for deposited titanium nitride thin film and its influence, Proc. of SPIE, Vol. 9068, 90680H (2013), doi: 10.1117/12.2053929.

[14] J. A. Montes de Oca Valero et al., Low temperature, fast deposition of metallic titanium nitride films using plasma activated reactive evaporation, J. Vac. Sci. Technol., Vol. A 23, No. 3, pp. 393-400 (2005).

[15] S. Prayakarao et al., Gyroidal titanium nitride as nonmetallic metamaterial, Opt Mater Express, Vol. 5, No. 6, pp. 1316-1322 (2015), doi:10.1364/OME.5.001316

[16] H. Van Bui, Atomic layer deposition of TiN films: growth and electrical behavior down to sub-nanometer scale, PhD. Thesis − University of Twente, Enschede, the Netherlands (2013). ISBN: 978-90-365-3484-0, doi: 10.3990/1/9789036534840.

[17] J. M. Lackner et al., Pulsed laser deposition: a new technique for deposition of amorphous SiOx thin films, Surf and Coat Technol., Vol. 163-164, pp. 300-305 (2003).

[18] K. Obata et al., TiN growth by hybrid radical beam-PLD for Si barrier metal, Proc. of SPIE, Vol. 3933, pp.166-173 (2000).

[19] T. Ikegami et al., Effect of high voltage pulses on plasma plume in TiN deposition by PLD method, T. IEE Japan, Vol. 119-A, No. 6, pp. 860-865 (1999).

[20] H. Guo et al., Microstructures and properties of titanium nitride films prepared by pulsed laser deposition at different substrate temperatures, Appl. Surf Sci., Vol. 357, pp. 473-478 (2015).

[21] S. H. Kim et al., Structure and mechanical properties of titanium nitride thin films grown by reactive pulsed laser deposition, J Ceram Process Res., Vol. 10, No. 1, pp. 49-53 (2009).

[22] Z. P. Wang, et al., Growth of preferentially-oriented AlN films on amorphous substrate by pulsed laser deposition, Phys. Lett., Section A General Atom Solid State Phys., Vol. 375, No. 33, pp. 3007-3011 (2011).

[23] K. Jagannadham et al., Structural characteristics of AlN films deposited by pulsed laser deposition and reactive magnetron sputtering: a comparative study, J. Vac. Sci. Technol., Vol. A 16(5), pp. 2804-2815 (Sep/Oct 1998).

[24] S. Adachi, The Handbook on optical constants of metals, World Scientific Publishing Co. Pte. Ltd. 5 Toh Tuck Link, Singapore 596224. ISBN: 978-981-4405-94-2 (2012).

[25] E. Pascual et al., Surface reflectivity of TIN thin films measured by spectral ellipsometry, Surf Sci., Vol. 251/252, pp. 200-203 (1991).

[26] K. Postava et al., Optical characterization of TiN/SiO2(1000 nm)/Si system by spectroscopic ellipsometry and reflectometry, Appl. Surf. Sci., Vol. 175-176, pp. 270-275 (2001).

[27] J. Pflünger et al., Dielectric properties of TiCx, TiNx, VCx, and VNx from 1.5 to 40 eV determined by electron-energy-loss spectroscopy, Phys. Rev. B, Vol. 30, No. (3), pp. 1155-1163 (1984).

[28] K. Murai, Y. Oshikane et al., Design and fabrication of active spectral filter with metal-insulator-metal structure for visible light communication, Proc. SPIE, Vol. 8632, 863223 (2013).

[29] Y. Oshikane et al., 3D-FEM analysis of SPP excitation through nanoholes in asymmetric metal-insulator-metal structure at tip of circular truncated conical fiber, Proc. SPIE, Vol. 9163, 916317 (2014).

[30] J. I. Roh et al., Homo-epitaxial growth of 3C-SiC(100) thin films on SiC/Si substrate treated by chemical mechanical polishing, J. Korean Phys. Soc., Vol. 43, No. 1, pp. 96-101 (July 2003).

[31] S. S. Menon et al., Comparison of the Ti/TiN/AlCu/TiN stack with TiN/AlCu/Ti/TiN stack for application in ULSI metallization, Proc. of SPIE, Vol. 2875, pp. 322-333 (1996).

[32] K. Thamaphat et al., Phase characterization of TiO_2 powder by XRD and TEM, J. Kasetsart (Nat. Sci.), Vol. 42, pp. 357-361 (2008).

[33] D. Jaeger et al, J. Electron Spectrosc. Relat. Phenom., Vol. 185, pp. 523-534 (2012).

[34] N. C. Saha et al., Titanium nitride oxidation chemistry: an x-ray photoelectron spectroscopy study, J. Appl. Phys., Vol. 72, 1 (1992).

[35] N. Jiang et al., XPS study for reactively sputtered titanium nitride thin films deposited under different substrate bias, Physica B, Vol. 352, pp. 118-126 (2004).

[36] http://www.xpsfitting.com/2009/03/titanaium-nitride.html.

[37] http://xpssimplified.com/elements/titanium.php.

[38] F. H. Lu et al., XPS analyses of TiN films on Cu substrates after annealing in the controlled atmosphere, Thin Solid Films, Vol. 355-356, pp. 374-379 (1999).

[39] XPST 1.1 (X-ray photoelectron spectroscopy tools version 1.1 for Igor Pro) which is put on http://www.igorexchange.com/project/XPStools.

IntechOpen